Desulphurisation of dibenzothiophene and 4,6 – dimethyl dibenzothiophene via enhanced hydrogenation reaction route using RePd–TiO_2/SiO_2 aerogel catalysts: Kinetic parameters estimation and modelling

Dragana Prokić-Vidojević[1], Sandra B. Glišić[2], Radojica Pešić[2] and Aleksandar M. Orlović[2]

[1]*Military Technical Institute (VTI), Ratka Resanovića 1, 11132 Belgrade, Serbia*
[2]*University of Belgrade, Faculty of Technology and Metallurgy, Karnegijeva 4, 11000 Belgrade, Serbia*

Abstract

Re/Pd-TiO_2/SiO_2 aerogel catalysts were synthesized by using a sol-gel method and supercritical drying in excess solvent and investigated in the reaction of hydrodesulphurisation (HDS) of dibenzothiophene (DBT) and 4,6-dimethyl dibenzothiophene (4,6-DMDBT). Both Re/Pd catalysts, obtained with and without the use of mesitylene in the synthesis step, have shown increased conversions of up to 70 % in the desulphurization of 4,6-DMDBT, when compared to conventional Co/Mo hydroprocessing catalysts. This observation is of importance for conversion of highly refractory 4,6-DMDBT and hydroprocessing to produce ultra-low sulphur diesel fuels, ULSD. In order to quantify the extent of desulphurisation, which proceeds via a hydrogenation route, conversions of DBT and 4,6-DMDBT along with evolution of reaction products characteristic for the direct desulphurisation route and the hydrogenation route were monitored by using a gas chromatography–mass spectrometry (GC-MS) analytical technique. The reaction was performed at 630 K and 6 MPa in a batch catalytic reactor. The experimental results were used in the Hougen-Watson kinetic model describing DBT and 4,6-DMDBT desulphurisation on σ and τ active sites. Kinetic parameters of this complex catalytic kinetics were determined by using a Genetic Algorithm method and minimum deviation function. Values of calculated kinetic parameters and values of the ratio of 3-methylcyclohexyltoluene (MCHT and dimethyl biphenyl (DMBPH) expressed as the MCHT/(MCHT+DMBPH) ratio ranging between 0.66 and 0.94, have confirmed that the hydrogenation route is the dominant route for desulphurisation of 4,6-DMDBT.

Keywords: Aerogel hydrodesulphurisation catalysts; hydrodesulphurisation; 4,6-DMDBT; Hougen-Watson kinetic model; kinetic and adsorption parameters.

Available on-line at the Journal web address: http://www.ache.org.rs/HI/

ORIGINAL SCIENTIFIC PAPER

UDC: 666.762.12:549.514.5:54.062

Hem. Ind. **76(3)** 135-145 (2022)

1. INTRODUCTION

Production of clean transportation fuels is becoming considerable challenge due to increased availability of heavier feedstock and depleted supply of light feedstock, which results in the continuous increase in molecular weight of available petroleum. Thus, the development of highly active hydrotreating catalysts for upgrading the heavy and sulphur-rich feedstock became inevitably important. This need was even more compelling in the view of recent environmental regulations, placing the current limit for sulphur content in diesel fuel down to below 10 ppm [1]. Decreasing the sulphur content to these levels is very difficult since sulphur compounds that remain after the conventional hydrodesulphurization (HDS) process are highly refractory [1]. Difficulties are encountered with dibenzotiphenes, especially its substituted derivative 4,6-dimethyldibenzitiophene (4,6-DMDBT) [2,3]. Substitute methyl groups cause considerable steric hindrance thereby making sulphur atom inaccessible to the active catalyst surface and hydrogen reactant. Deep HDS could be improved by the development of new state-of-the-art catalysts, capable of achieving efficient clean fuel production [3,4].

Corresponding authors: Sandra B. Glišić, University of Belgrade, Faculty of Technology and Metallurgy, Karnegijeva 4, 11000 Belgrade, Serbia, Tel: +381 113303707; fax: +381 113370378

E-mail: : sglisic@tmf.bg.ac.rs

Paper received: 14 January 2022; Paper accepted: 10 April 2022; Paper published: 17 July 2022.
https://doi.org/10.2298/HEMIND220114008P

Deep HDS requires supports with high surface areas, enhanced pore sizes, higher fraction of mesopores and small macropores, larger pore volumes allowing increased exposure of active sites and better dispersion of active components and their availability to large sulphur molecules. Due to these reasons, the conventionally used γ-alumina (γ-Al_2O_3) support is a far less efficient option compared to other supports like highly porous silicas, which are increasingly attractive [5-10]. Their main advantages for use as catalyst supports are: high surface areas of about 600-1300 m^2/g and huge pore volumes; uniform topology providing high dispersion of metal nanoparticles and easy access of the reactants to the active sites; excellent mechanical properties and hydrothermal stability for demanding reaction conditions. Further HDS improvement was reported with the incorporation of heteroatoms: Al, Ti and Zr ions, into frameworks of highly porous silica materials [3,11-14] which increased pore diameters and facilitated hydrogenation of benzene ring. A Ti-containing catalyst was found to be 30 % more active than the conventional industrial catalyst and 50% more active than the Ti-free catalyst [15]. In order to achieve desired catalytic and textural characteristics of HDS catalysts the choice of the preparation method is very important [16-19]. Improvements in specific surface area [18,19], pore volume, homogenous formation of hetero-linkages and development of appropriate surface acid sites [16,17] was reported by using a sol-gel method whereas higher acidity in the sol-gel samples was attributed to higher density of hetero-linkages formed [18,19]. To overcome the problem of deteriorated textural properties caused by conventional drying methods (collapse of the formed gel structure and reduction of mesoporosity by the increasing fraction of micropores leading to decreased surface areas) [20,21], a supercritical drying method (SCD) can be applied to obtain aerogels [22-24]. SCD can be performed for solvent removal by solvent phase change to supercritical (SC) fluid, followed by solvent evacuation from the gel network by applying transition from supercritical fluid to gas. Aerogels produced by supercritical drying typically have high porosities (50-99 vol%), lower microporosity, higher surface areas and can yield highly porous amorphous mixed oxide aerogels [22-24]. Besides advantageous textural properties, the choice of active phase is equally important in order to design a highly active catalyst for "deep HDS". Numerous studies have confirmed high activity of nonconventional sulphides, such as Re, Rh or Ru [25-28]. The way to further enhance activity of ReS_2 can be achieved through understanding of the HDS reaction mechanism of 4,6-DMDBT and potential for the use of noble metals as promoters. This potential is based on the exceptional properties of Pd, Pt and Ru, suitable for hydrogen spillover in aromatics hydrogenation, necessary for deep HDS [29-33].

The sol-gel synthesis method and supercritical drying of the obtained gels, for RePd supported on Ti-HMS (Ti incorporated in highly mesoporous silica), were previously investigated as HDS catalysts [34]. The sol-gel method and supercritical drying were found to result in amorphous aerogels with a relatively high degree of uniformity of both supports and active phases [34,35]. Catalytic activities of the obtained aerogels and a commercial Co/Mo catalyst in HDS of DBT were not significantly different [34]. However, large differences were observed in HDS of 4,6-DMDBT since all Re/Pd-TiO_2/SiO_2 aerogel catalysts were considerably more active than Co/Mo-Al_2O_3/SiO_2 aerogel catalysts and a Co/Mo on γ-alumina commercial HDS catalyst, alike [34]. Conversion of 4,6-DMDBT was found to be 70 % higher for RePd aerogel catalysts obtained by using mesitylene addition (RePd MA) and 64 % higher for RePd aerogel catalysts obtained without mesitylene addition (RePd A), when compared to conversion achieved by using a commercial Co/Mo catalyst [34].

Kinetic modelling of HDS reactions has been carried out by several researchers [36–47]. The Langmuir-Hinshelwood, also well known as the Hougen−Watson mechanism, has been reported to suitably describe the HDS reactions [20–22]. Hougen−Watson rate equations for hydrogenolysis and hydrogenation of dibenzothiophenes to bicyclohexyl through several steps, were developed by Froment and co-workers [36-38]. Two different types of active sites were considered: σ sites for hydrogenolysis and τ sites for hydrogenation. The surface reaction between adsorbed reactants and two competitively adsorbed hydrogen atoms was found to be the rate-determining step for both types of reaction. Actually, the HDS mechanism of substituted aromatic sulphur compounds involves a pre-hydrogenation step (HYD) before desulphurization [29,30]. This is the key step in order to remove the steric hindrance of the substituents, contrary to the non-sterically hindered compounds that are straightforwardly desulphurised *via* a direct desulphurization (DDS) pathway [33]. Consequently, for well-established catalytic formulations (*e.g*. CoMo, NiMo) even with excellent DBT HDS properties, HYD efficiency becomes an obstacle for substituted DBTs like 4,6-DMDBT. The present research is focused on investigating the kinetics of the simultaneous HDS of two sulphur containing model compounds (DBT and

4,6-DMDBT), using RePd MA and RePd A catalysts. The novelty of this study is the approach which includes DDS and HYD pathways for all reacting species in the kinetic model.

Thus, the objective of the study is to investigate the hydrodesulphurisation (HDS) of dibenzothiophene (DBT) and 4,6-dimethyl dibenzothiophene (4,6-DMDBT) for Re/Pd-TiO_2/SiO_2 aerogel catalysts, obtained with and without the use of mesitylene in the synthesis step. Gas chromatography–mass spectrometry (GC-MS) was used to quantify concentrations of reactants and emerging reaction products over time, at 630 K and 60 bar in a batch catalytic reactor. Based on the experimental data, the Hougen-Watson kinetic model for desulphurisation of DBT and 4,6-DMDBT on σ and τ active sites was developed. Kinetic parameters of the model were determined in a procedure based on the use of the Genetic Algorithm (GA) method and minimum deviation function.

2. EXPERIMENTAL

2. 1. Catalysts used in catalytic HDS tests

Re/Pd-TiO_2/SiO_2 aerogel catalysts were synthesized by using a sol-gel method and supercritical drying in excess solvent as described in previously published work [34,35]. The Re/Pd-TiO_2/SiO_2 catalysts were obtained by using two different pathways of the sol-gel method, the pathway which applies mesitylene in the sol phase as the additional template for enhancement of the mesopore region (RePd MA catalyst) and the pathway without mesitylene (RePd A catalyst), while in both pathways supercritical drying with excess solvent was applied. Structural and textural properties of the obtained aerogel HDS catalysts and TiO_2/SiO_2 supports were investigated and reported previously [34].

2. 2. Hydrodesulphurisation (HDS) reaction tests of dibenzothiophene (DBT) and 4,6-dimethyldibenzothiophene (4,6-DMDBT) - catalytic activity of the RePd A and RePd MA catalysts

Re/Pd-TiO_2/SiO_2 aerogel catalyst (RePd A) and Re/Pd-TiO_2/SiO_2 aerogel catalyst obtained by using mesitylene during sol-gel synthesis (RePd MA) were investigated by performing HDS of DBT and 4,6-DMDBT in a high pressure stirred-batch reactor (Autoclave Engineers BTRS Jr, Division of Snap-title, Inc., Erie, PA, USA). Prior to the reaction, each catalyst (0.84 g) was activated by sulphidation with carbon disulphide (7 cm^3, grade, producer, country) at 603 K and 35 bar of H_2 during 4 h. The DBT and 4,6-DMDBT HDS activity tests were performed in a 300 cm^3 stirred-batch reactor at 603 K and 6 MPa total pressure, for 6 h. All reaction tests were performed with the 100 ml solution of DBT (0.8 g) and 4,6-DMDBT (0.10 g) in the (1:1 v/v) mixture of n-hexadecane (grade, producer, country) and n-dodecane (grade, producer, country) leading to the total elemental sulphur concentration of 2000 ppm weight based. The reaction was monitored by withdrawing samples (2 ml) at 0.25, 0.5, 1, 1.5, 2, 3, 4, 5 and 6 h of reaction time. All experiments were done in 2 repetitions.

2. 3. Product analysis

Quantitative analysis of the reactants (DBT and 4,6-DMDBT) and products was carried out using Shimadzu GC-2010 Plus, MS QP 2020 instrument (Shimadzu, Japan), equipped with a capillary column sh-rtx-5 (30 m × 0.25 μm × 0.25 mm) using a temperature program starting from 333 to 503 K (heating rate of 6 K/min). GC-MS quantification was applied on samples withdrawn from the liquid phase using calibration lines obtained with DBT and 4,6-DMDBT. Identification of mass spectra peaks was performed using the scientific library NIST11s. Quantities and concentrations of hydrogen sulphide in both phases (vapour and liquid) were calculated from the material balance of sulphur containing reactants (DBT and 4,6-DMDBT) and vapour-liquid equilibrium calculation using the Peng-Robinson equation of state. Hydrogen sulphide concentration in the liquid phase is relevant for the kinetic model and phase distribution is given by K_{eq} values in Eq. 19.

3. KINETIC MODEL AND DETERMINATION OF KINETIC PARAMETERS

Kinetic model describing HDS of DBT and 4,6-DMDBT, shown in Figure 1, was employed to develop the kinetic model equations, experimental reactor material balance equations and optimisation technique for determination of kinetic parameters.

The removal of sulphur from organic sulphur compounds can occur through two pathways: direct desulphurization (DDS) by C-S bond cleavage without affecting the aromatic ring and hydrogenation of the aromatic ring (HYD) prior to the cleavage of C-S bond [36-41]. Both reaction pathways are generally believed to occur at separate catalytic sites. The DDS pathway is economical because this route consumes lower amounts of hydrogen. Both routes, the HYD of DBT and DDS of DBT yield biphenyl (BPH), while the HYD route produces intermediates such as tetrahydrodibenzothiophene (THDBT) and hexahydrodibenzothiophene (HHDBT), that rapidly convert to cyclohexyl benzene (CHB) and further to bicycle hexyl (BCH). Similarly, the DDS of 4,6-DMDBT produces 3,3'-dimethyl biphenyl (DMBPH), whereas the HYD pathway results in 3-methylcyclohexyltoluene (MCHT) and furthermore to 3,3-dimethyl bicycle hexyl (DMBCH). Figure 1 shows simple schemes for the reaction pathways of the DBT and 4,6-DMDBT. The transitional compounds produced through HDS of DBT and 4,6-DMDBT *via* the HYD routes were observed in negligible amounts whereas the major products were CHB and MCHT from the HDS of DBT and 4,6- DMDBT, respectively.

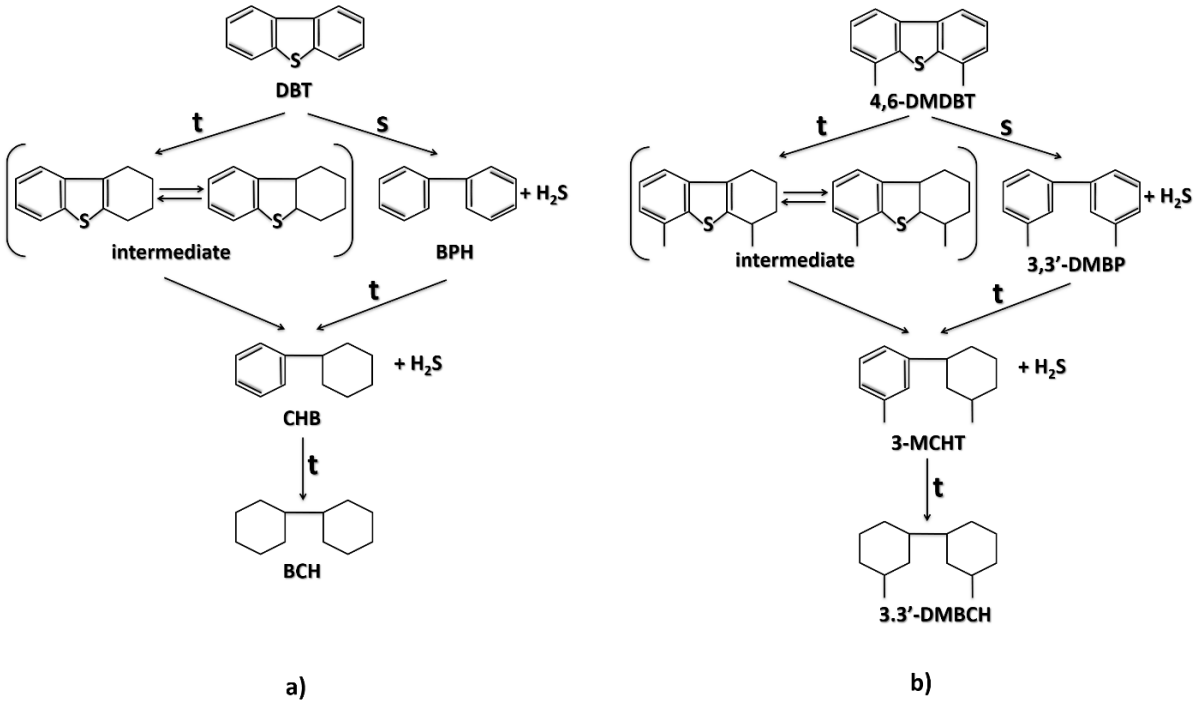

Figure 1. Kinetic model describing HDS of a) DBT and b) 4,6-DMDBT on σ and τ active sites

A Hougen−Watson based kinetic model was developed based on the reaction network presented in Figure 1 that included the simultaneous HDS reactions supported by the experimental results. Based on the kinetic model scheme the set of differential equations representing material balances for each compound involved in the reaction was developed and shown in Eq. 1-19:

DBT:

$$-r_{DBT}^{\sigma} = \frac{k^{\sigma}_{DBT} K^{\sigma}_{H} K^{\sigma}_{DBT} c_{DBT} c_{H_2}}{\left(1 + K^{\sigma}_{DBT} + c_{DBT}\sqrt{K^{\sigma}_{H} c_{H_2}} + K^{\sigma}_{BPH} c_{BPH} + k^{\sigma}_{H_2S} c_{H_2S} + K^{\sigma}_{DMDBT} c_{DMDBT} + K^{\sigma}_{DMBP} c_{DMBP}\right)^3} \quad (1)$$

$$-r_{DBT}^{\tau} = \frac{k^{\tau}_{DBT} K^{\tau}_{H} K^{\tau}_{DBT} c_{DBT} c_{H_2}}{\left(1 + K^{\tau}_{DBT} c_{DBT} + \sqrt{K^{\tau}_{H} c_{H_2}} + K^{\tau}_{BPH} c_{BPH} + K^{\tau}_{CHB} c_{CHB} + K^{\tau}_{BCH} c_{BCH} + K^{\tau}_{DMDBT} c_{DMDBT} + K^{\tau}_{DMBP} c_{DMBP} + K^{\tau}_{MCHT} c_{MCHT} + K^{\tau}_{DMBCH} c_{DMBCH}\right)^3} \quad (2)$$

$$-r_{BPH}^{\tau} = \frac{k^{\tau}_{BPH} K^{\tau}_{H} K^{\tau}_{BPH} c_{BPH} c_{H_2}}{\left(1 + K^{\tau}_{DBT} c_{DBT} + \sqrt{K^{\tau}_{H} c_{H_2}} + K^{\tau}_{BPH} c_{BPH} + K^{\tau}_{CHB} c_{CHB} + K^{\tau}_{BCH} c_{BCH} + K^{\tau}_{DMDBT} c_{DMDBT} + K^{\tau}_{DMBP} c_{DMBP} + K^{\tau}_{MCHT} c_{MCHT} + K^{\tau}_{DMBCH} c_{DMBCH}\right)^3} \quad (3)$$

$$r_{CBH}^{\tau} = -r_{DBT}^{\tau} - r_{BPH}^{\tau} - \frac{k^{\tau}_{CHB} K^{\tau}_{H} K^{\tau}_{CHB} c_{CHB} c_{H_2}}{\left(1 + K^{\tau}_{DBT} c_{DBT} + \sqrt{K^{\tau}_{H} c_{H_2}} + K^{\tau}_{BPH} c_{BPH} + K^{\tau}_{CHB} c_{CHB} + K^{\tau}_{BCH} c_{BCH} + K^{\tau}_{DMDBT} c_{DMDBT} + K^{\tau}_{DMBP} c_{DMBP} + K^{\tau}_{MCHT} c_{MCHT} + K^{\tau}_{DMBCH} c_{DMBCH}\right)^3} \quad (4)$$

$$r_{BCH}^{\tau} = -\frac{k^{\tau}_{CHB} K^{\tau}_{H} K^{\tau}_{CHB} c_{CHB} c_{H_2}}{\left(1 + K^{\tau}_{DBT} c_{DBT} + \sqrt{K^{\tau}_{H} c_{H_2}} + K^{\tau}_{BPH} c_{BPH} + K^{\tau}_{CHB} c_{CHB} + K^{\tau}_{BCH} c_{BCH} + K^{\tau}_{DMDBT} c_{DMDBT} + K^{\tau}_{DMBP} c_{DMBP} + K^{\tau}_{MCHT} c_{MCHT} + K^{\tau}_{DMBCH} c_{DMBCH}\right)^3} \quad (5)$$

DMDBT:

$$-r_{DMDBT}^{\sigma} = \frac{k^{\sigma}_{DMDBT} K^{\sigma}_{H} K^{\sigma}_{DMDBT} c_{DMDBT} c_{H_2}}{\left(1 + K^{\sigma}_{DBT} + c_{DBT} \sqrt{K^{\sigma}_{H} c_{H_2}} + K^{\sigma}_{BPH} c_{BPH} + k^{\sigma}_{H_2S} c_{H_2S} + K^{\sigma}_{DMDBT} c_{DMDBT} + K^{\sigma}_{DMBP} c_{DMBP}\right)^3} \quad (6)$$

$$-r_{DMDBT}^{\tau} = \frac{k^{\tau}_{DMDBT} K^{\tau}_{H} K^{\tau}_{DMDBT} c_{DMDBT} c_{H_2}}{\left(1 + K^{\tau}_{DBT} c_{DBT} + \sqrt{K^{\tau}_{H} c_{H_2}} + K^{\tau}_{BPH} c_{BPH} + K^{\tau}_{CHB} c_{CHB} + K^{\tau}_{BCH} c_{BCH} + K^{\tau}_{DMDBT} c_{DMDBT} + K^{\tau}_{DMBP} c_{DMBP} + K^{\tau}_{MCHT} c_{MCHT} + K^{\tau}_{DMBCH} c_{DMBCH}\right)^3} \quad (7)$$

$$-r_{DMBH}^{\tau} = \frac{k^{\tau}_{DMBP} K^{\tau}_{H} K^{\tau}_{DMBP} c_{DMPHP} c_{H_2}}{\left(1 + K^{\tau}_{DBT} c_{DBT} + \sqrt{K^{\tau}_{H} c_{H_2}} + K^{\tau}_{BPH} c_{BPH} + K^{\tau}_{CHB} c_{CHB} + K^{\tau}_{BCH} c_{BCH} + K^{\tau}_{DMDBT} c_{DMDBT} + K^{\tau}_{DMBP} c_{DMBP} + K^{\tau}_{MCHT} c_{MCHT} + K^{\tau}_{DMBCH} c_{DMBCH}\right)^3} \quad (8)$$

$$r_{MCHT}^{\tau} = -r_{DMDBT}^{\tau} - r_{DMBPPH}^{\tau} - \frac{k^{\tau}_{MCHT} K^{\tau}_{H} K^{\tau}_{MCHT} c_{MCHT} c_{H_2}}{\left(1 + K^{\tau}_{DBT} c_{DBT} + \sqrt{K^{\tau}_{H} c_{H_2}} + K^{\tau}_{BPH} c_{BPH} + K^{\tau}_{CHB} c_{CHB} + K^{\tau}_{BCH} c_{BCH} + K^{\tau}_{DMDBT} c_{DMDBT} + K^{\tau}_{DMBP} c_{DMBP} + K^{\tau}_{MCHT} c_{MCHT} + K^{\tau}_{DMBCH} c_{DMBCH}\right)^3} \quad (9)$$

$$r_{DMBCH}^{\tau} = -\frac{k^{\tau}_{MCHT} K^{\tau}_{H} K^{\tau}_{MCHT} c_{MCHT} c_{H_2}}{\left(1 + K^{\tau}_{DBT} c_{DBT} + \sqrt{K^{\tau}_{H} c_{H_2}} + K^{\tau}_{BPH} c_{BPH} + K^{\tau}_{CHB} c_{CHB} + K^{\tau}_{BCH} c_{BCH} + K^{\tau}_{DMDBT} c_{DMDBT} + K^{\tau}_{DMBP} c_{DMBP} + K^{\tau}_{MCHT} c_{MCHT} + K^{\tau}_{DMBCH} c_{DMBCH}\right)^3} \quad (10)$$

Material balance equations:

DBT: $$-\frac{dC_{DBT}}{dt} = -r_{DBT}^{\sigma} - r_{DBT}^{\tau} \quad (11)$$

BPH: $$\frac{dC_{BPH}}{dt} = -r_{DBT}^{\sigma} - r_{BPH}^{\tau} \quad (12)$$

CHB: $$\frac{dC_{CHB}}{dt} = -r_{DBT}^{\tau} - r_{BPH}^{\tau} - \frac{k^{\tau}_{CHB} K^{\tau}_{H} K^{\tau}_{CBH} c_{CBH} c_{H_2}}{\left(1 + K^{\tau}_{DBT} c_{DBT} + \sqrt{K^{\tau}_{H} c_{H_2}} + K^{\tau}_{BPH} c_{BPH} + K^{\tau}_{CHB} c_{CHB} + K^{\tau}_{BCH} c_{BCH} + K^{\tau}_{DMDBT} c_{DMDBT} + K^{\tau}_{DMBP} c_{DMBP} + K^{\tau}_{MCHT} c_{MCHT} + K^{\tau}_{DMBCH} c_{DMBCH}\right)^3} \quad (13)$$

BCH: $$\frac{dC_{BCH}}{dt} = r_{BCH}^{\tau} \quad (14)$$

DMDBT: $$-\frac{dC_{DMDBT}}{dt} = -r_{DMDBT}^{\sigma} - r_{DMDBT}^{\tau} \quad (15)$$

DMBPH: $$\frac{dC_{DMBP}}{dt} = -r_{DMBP}^{\sigma} - r_{DMBP}^{\tau} \quad (16)$$

MCHT: $$\frac{dC_{MCHT}}{dt} = -r_{DMDBT}^{\tau} - r_{DMBP}^{\tau} - \frac{k^{\tau}_{MCHT} K^{\tau}_{H} K^{\tau}_{MCHT} c_{MCHT} c_{H_2}}{\left(1 + K^{\tau}_{DBT} c_{DBT} + \sqrt{K^{\tau}_{H} c_{H_2}} + K^{\tau}_{BPH} c_{BPH} + K^{\tau}_{CHB} c_{CHB} + K^{\tau}_{BCH} c_{BCH} + K^{\tau}_{DMDBT} c_{DMDBT} + K^{\tau}_{DMBP} c_{DMBP} + K^{\tau}_{MCHT} c_{MCHT} + K^{\tau}_{DMBCH} c_{DMBCH}\right)^3} \quad (17)$$

DMBCH: $$\frac{dC_{DMBCH}}{dt} = \frac{k^{\tau}_{MCHT} K^{\tau}_{H} K^{\tau}_{MCHT} c_{MCHT} c_{H_2}}{\left(1 + K^{\tau}_{DBT} c_{DBT} + \sqrt{K^{\tau}_{H} c_{H_2}} + K^{\tau}_{BPH} c_{BPH} + K^{\tau}_{CHB} c_{CHB} + K^{\tau}_{BCH} c_{BCH} + K^{\tau}_{DMDBT} c_{DMDBT} + K^{\tau}_{DMBP} c_{DMBP} + K^{\tau}_{MCHT} c_{MCHT} + K^{\tau}_{DMBCH} c_{DMBCH}\right)^3} \quad (18)$$

H_2S: $$\frac{dC_{H_2S}}{dt} = \frac{1}{K_{eq}}\left(-r_{DBT}^{\sigma} - r_{DBT}^{\tau} - r_{DMDBT}^{\sigma} - r_{DMDBT}^{\tau}\right) \quad (19)$$

The total of 23 parameters contained in the Hougen-Watson kinetic model (k_i – kinetic constants and K_i – adsorption coefficients, listed in Eqs. (1)–(19)) were determined using an optimization technique in the MATLAB software (MathWorks, USA). The technique used is a combination of Genetic Algorithm GA and Fminsearch methods as a hybrid optimization technique (GA-Fminsearch) that determines parameters in a way to minimize the deviation (Error) between the model and experimental data, Eq. (20):

$$\text{Error} = \sum_i \frac{\sum_j \left| c_{i,j}^{\text{Exp}} - c_{i,j}^{\text{Model}} \right|}{c_{i,j}^{\text{Exp}}} \quad (20)$$

Genetic Algorithm (GA) is an optimization method which is using operators Selection, Crossover, Mutation, and Sampling, and finds the global minimum at the end [48-50]. One of the superiorities of GA over classical optimization techniques is that it does not need any additional information, such as derivatives, about the target function [49], searching from population of points, handling coded values of the problem parameters, and using probabilistic transition operators [50,51]. By combining GA with a local search method, such as Fminsearch, finding the exact optimum point becomes the less time-consuming process. Fminsearch is an optimization technique that determines the minimum of an unconstrained multivariable function by using a derivative-free method starting from an initial guess, employing the Nelder-Mead simplex algorithm [52], and finding the local minimum corresponding to the initial guess. Fminsearch converges faster to a solution than GA does, but it needs a suitable initial guess to obtain the global minimum without being trapped in the local minimum. The role of GA in the hybrid GA-Fminsearch technique is finding the initial guess of the reactions' constants.

4. RESULTS AND DISSCUSION

Testing of catalytic activity of RePd A and RePd MA catalysts on TiO_2/SiO_2 supports was performed at 630 K and 60 bar in a batch catalytic reactor. Concentrations of all relevant species were determined in order to quantify species evolving through DDS and HYD reaction pathways, so to generate sufficient experimental data, which can be used in determination of kinetic parameters. Values of concentrations for reactants and all reaction products are shown in Table 1 (average absolute deviations of two runs are: 0.124 for RePd A and 0.107 for RePd MA).

Table 1. Experimental data of concentration profiles along the reaction time for reactants and reaction products

RePd A catalyst									
Time, h	Concentration, mol dm^{-3}								
	DBT	BPH	CHB	BCH	DMDBT	DMBPH	MCHT	DMBCH	H_2S*
0	0.0339	0	0	0	0.00368	0	0	0	0
0.25	0.02702	0.00625	0.00063	0	0.00342	0.00004	0.0002	0.00002	0.00293
0.5	0.02649	0.00621	0.00075	0.00045	0.00298	0.00008	0.00031	0.0003	0.00332
1	0.02299	0.0092	0.00115	0.00057	0.00287	0.00014	0.00047	0.00019	0.0048
1.5	0.02132	0.01062	0.00138	0.00058	0.00265	0.00022	0.00061	0.00021	0.00557
2	0.0144	0.01599	0.00256	0.00095	0.0025	0.00025	0.00063	0.0003	0.00847
3	0.01111	0.0185	0.00333	0.00095	0.0021	0.00029	0.0006	0.00069	0.00998
4	0.00898	0.02016	0.00383	0.00093	0.00184	0.00026	0.00044	0.00114	0.01095
5	0.00608	0.02182	0.0048	0.0012	0.00125	0.00022	0.00028	0.00193	0.01238
6	0.00521	0.02212	0.00531	0.00127	0.00099	0.00013	0.00016	0.0024	0.01285
RePd MA catalyst									
Time, h	Concentration, mol dm^{-3}								
	DBT	BPH	CHB	BCH	DMDBT	DMBPH	MCHT	DMBCH	H_2S
0	0.0339	0	0	0	0.00368	0	0	0	0
0.25	0.0339	0	0	0	0.00305	0.00009	0.00016	0.00038	0.00026
0.5	0.03083	0.00188	0	0.00119	0.00261	0.0002	0.00031	0.00056	0.0017
1	0.02799	0.00286	0.00021	0.00284	0.00239	0.00025	0.0004	0.00064	0.00295
1.5	0.02417	0.00522	0.0005	0.00401	0.00236	0.00026	0.00047	0.0006	0.00453
2	0.01854	0.00918	0.00138	0.0048	0.00195	0.00025	0.00057	0.00091	0.007
3	0.01598	0.00974	0.00455	0.00363	0.00173	0.00022	0.00074	0.00099	0.00814
4	0.0148	0.00983	0.00593	0.00334	0.00151	0.00027	0.00084	0.00106	0.00871
5	0.00845	0.01098	0.01012	0.00435	0.0011	0.0004	0.00111	0.00106	0.01147

*Concentration of H_2S is in the liquid phase. Values were obtained by molar balance calculation and vapour – liquid equilibrium calculation using the Peng – Robinson Equation of State

The obtained experimental results, concentration profiles, were applied in the widely used Hougen-Watson kinetic model describing DBT and 4,6-DMDBT desulphurisation on σ and τ active sites, as shown above. Kinetic parameters of this complex catalytic kinetics were determined in a procedure using GA-Fminsearch method and minimum deviation function. The results of parameter estimation are reported in Table 2 and comparison of simulated and experimental data obtained with optimized constants are shown in Figure 2.

Table 2. Values of determined and optimized kinetic parameters and comparison with the same constants obtained by Froment and co-workers for a Co/Mo catalyst [36-38]

Kinetic and adsorption constants on σ and τ active sites	RePd A	RePd MA	Co/Mo catalyst recalculated constants for 603 K [36-38]
	Adsorption equilibrium constant, $m^3\ kmol^{-1}$		
K^{σ}_{BPH}	12.68	0.00	5.78
K^{σ}_{DMPP}	7.51	329.32	0
K^{τ}_{DMDBT}	9.08	2.12	1.09
K^{τ}_{MCHT}	25.72	40.14	NA
K^{σ}_{DBT}	2.74	0.82	75.69 constant value for all temperatures
K^{τ}_{DBT}	3.13	0.00	2.14
K^{τ}_{BPH}	3.20	13.51	0.95
K^{τ}_{CHB}	4.02	10.15	$K^{\tau}_{CHB}\ k^{\tau}_{CHB}$ (573 K) = 0.000339
K^{τ}_{DMBP}	14.33	25.17	0
K^{σ}_{DMDBT}	2.19	0.36	18.04
K^{τ}_{DMBCH}	0.19	24.05	NA
K^{τ}_{BCH}	0.00	2470.34	NA
K^{σ}_{H2S}	12.75	1.89	20.92
K^{σ}_{H}	0.13	3.17	0.216
K^{t}_{H}	0.00	2.42	0.00321
K_{eq} for H_2S	2.48	2.25	NA
	Kinetic constant, kmol $kg_{cat}^{-1}\ h^{-1}$		
k^{σ}_{DBT}	1.11	0.33	0.57
k^{τ}_{DBT}	2.15	0.33	2.14
k^{σ}_{DMDBT}	0.23	0.66	0.041
k^{τ}_{DMDBT}	3.07	0.63	46.12
k^{τ}_{BPH}	1.33	3.08	24.19
k^{τ}_{DMBP}	2.96	6.23	Not in the kinetic model
k^{τ}_{CHB}	2.96	2.83	$K^{\tau}_{CHB}\ k^{\tau}_{CHB}$ (573 K)= 0.000339
k^{τ}_{MCHT}	4.19	0.66	Not in the kinetic model
Error	0.1312	0.1435	Not known

The Figure 2 confirms that the concentrations of different species predicted by the Hougen−Watson based kinetic model closely match the experimentally determined values.

Results of test reactions for conversion of DBT and 4,6-DMDBT are shown in Figure 3, obtained by using the estimated kinetic parameters for RePd A and RePd MA catalyst. The Figure 3 also shows conversion of DBT and 4,6-DMDBT obtained by using kinetic parameters developed by the Froment group for a commercial Co/Mo catalyst [36-38] and recalculated for the same temperature of reaction (603 K). It is obvious that the calculated Co/Mo catalyst activity is quite high and comparable to those of aerogel catalysts. However, it should be noted that the kinetic parameters determined by the Froment group [36-38] were obtained in the different temperature interval (temperature range 513 – 593 K) and different pressure (7 MPa) than the one used in this work. The experimental hydrogen/hydrocarbon ratio (2.3 and 3.5) and catalyst/feed ratio (4.6 times more catalyst then in this research) were also different. The commercial Co/Mo catalyst activity in HDS of 4,6-DMDBT (conversion 62.4 mol.% after 6 h) is lower than activities

of the investigated aerogels (conversion 73.6 and 76.6 mol.% after 6 h respectively for RePd MA and RePd A) (Figure 3b), which is of significance for HDS of diesel oil fractions.

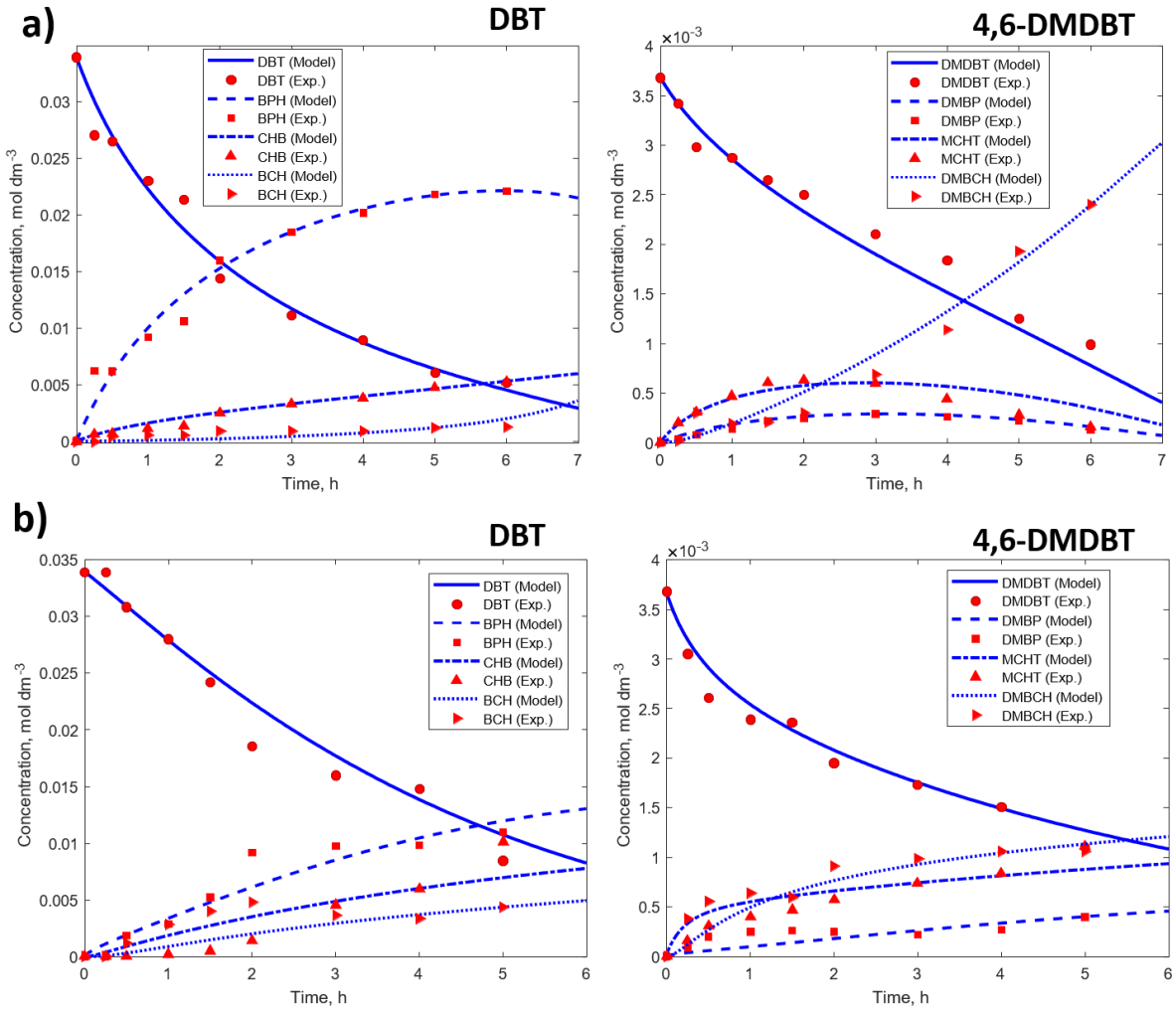

Figure 2. The experimental and simulated data obtained for hydrodesulphurization of DBT and 4,6-DMDBT using a) RePd A and b) RePd MA catalyst

High activity of RePd aerogels can be explained by, and attributed to, their unique properties. These advantageous properties are high surface area (848 $m^2 g^{-1}$ for RePd A and 643 $m^2 g^{-1}$ for RePd MA) and very high mesoporosity (volume of mesopores 0.466 $cm^3 g^{-1}$ for RePd A and 1.618 $cm^3 g^{-1}$ for RePd MA) as determined previously [34]. Also, mesopore fractions of 0.71 for RePd A and 0.55 for RePd MA [34] indicate high proportion of catalytically active surfaces. Texture was also characterized by the presence of large mesopores and small macropores (overall porosities are 0.656 $cm^3 g^{-1}$ for RePd A and 2.956 $cm^3 g^{=1}$ for RePd MA [34]) which are both expected to eliminate diffusional limitations and thus increase reaction rates. Good dispersion of RePd within the catalyst structure was evidenced resulting in higher concentrations of surface active sites [34]. Finally, the increased acidity of the titania-silica support which is the result of good Ti dispersion within the silica matrix [34] and high activity of the catalytically active Re/Pd phase [53] are contributing to the overall high activity of these aerogel catalysts.

Further insights into possible explanations for high activity of RePd aerogels could be found in the modification of the overall reaction pathway. As indicated in the introductory part of this study, an explanation could be associated with the exceptional properties of Pd which were found to be suitable for hydrogen spillover in hydrogenation of aromatics [29-32]. This is the critical step for deep HDS *via* a HYD route. As a result, highly active catalytic formulations with excellent DBT HDS activity (like CoMo with depleted HYD efficiency) can become relatively inactive for desulphurisation of 4,6-DMDBT.

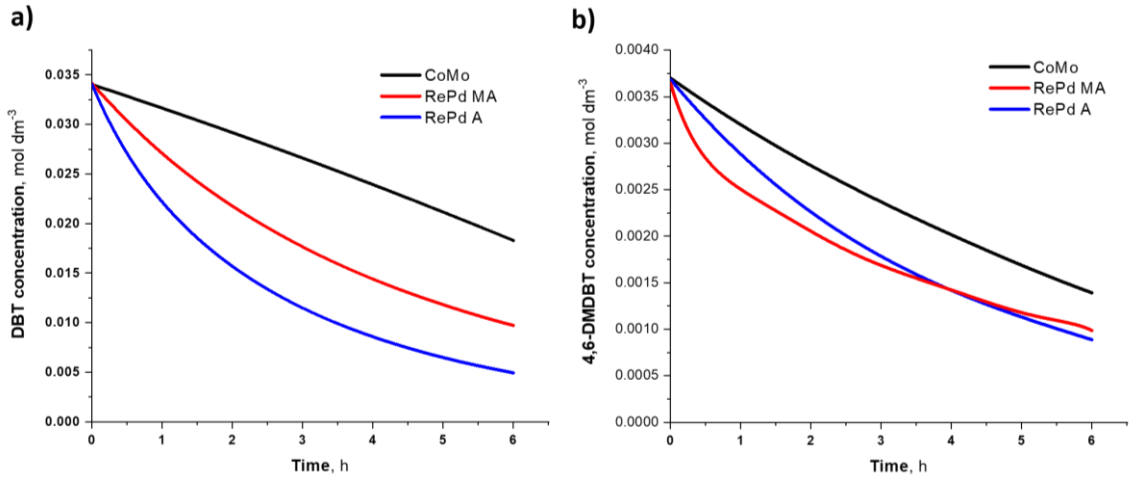

Figure 3. Predicted concentrations of a) DBT and b) 4,6-DMDBT over time in HDS for the investigated catalysts and a commercial catalyst Co/Mo based on the kinetic parameters in Table 2

Indication of the dominant reaction pathway for RePd catalysts was examined by GC-MS analysis of reaction products obtained in HDS of DBT. The selectivity towards CHB, expressed as CHB/(CHB+BP) ratio and MCHT expressed as MCHT/(MCHT+DMBPH), obtained by simulation based on using the obtained kinetic and adsorption constants during reaction (Table 2) are shown in Figure 4. It is interesting to observe that the CHB selectivity is considerably higher for RePd MA catalyst obtained with mesitylene addition than for the other two types of catalyst, RePd A without mesitylene addition and CoMo catalysts. Values of MCHT/(MCHT+DMBPH) ratio are significantly higher than the values of CHB/(CHB+BP) ratio, indicating overwhelming HYD activity in HDS of 4,6-DMDBT. A possible explanation might be found in a combination of RePd MA characteristics such as: large volume of mesopores, the shift of pore size distribution (PSD) to larger mesopores, slightly higher overall Pd/Re ratio and higher local Pd/Re ratios as compared to RePd A [34]. Some of these characteristics have been found to influence activity of RePd catalysts considerably [53] and could represent an opportunity for potential improvement of catalysts dedicated to various hydrogenation reactions, in particular hydrogenation of large molecules which are found in heavier petroleum fractions.

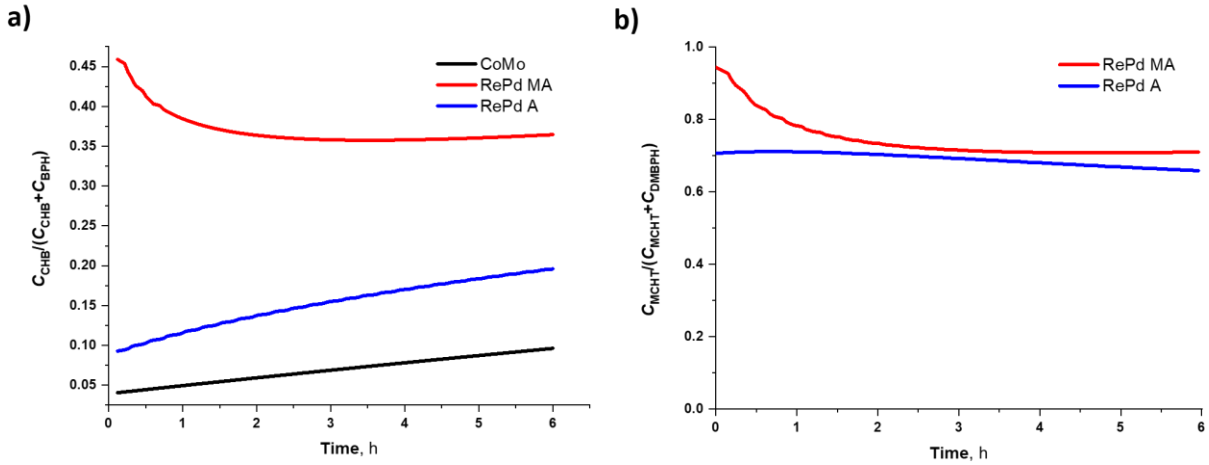

Figure 4. Predicted selectivity towards a) CHB expressed as CHB/(CHB+BP) and b) MCHT expressed as MCHT/(MCHT+DMBPH) in the HDS of DBT and 4,6-DMDBT for the investigated catalysts and a commercial catalyst Co/Mo based on the kinetic parameters in Table 2

5. CONCLUSION

Hydrodesulphurisation (HDS) of dibenzothiophene (DBT) and 4,6-dimethyl dibenzothiophene (4,6-DMDBT) by using Re/Pd catalysts (obtained with and without the use of mesitylene in the synthesis step) at 630 K and 6 MPa in a batch catalytic reactor was investigated in the present study. The Hougen-Watson kinetic model was applied to describe

desulphurisation of DBT and 4,6-DMDBT on σ and τ active sites and kinetic parameters were determined in a procedure based on using Genetic Algorithm (GA) method and minimum deviation function. Values of calculated kinetic parameters have shown that the hydrogenation route is the dominant route for desulphurisation of 4,6-DMDBT in the case of newly developed catalysts based on Re/Pd and highly mesoporous silica support with incorporated Ti. The obtained results were compared with predicted commercial Co/Mo catalyst activity in HDS of 4,6-DMDBT based on literature data indicating higher catalytic activities of the investigated Re/Pd aerogels. These findings are of potential significance for deep hydrodesulphurisation of diesel oil fractions. The most significant conclusion is that values of MCHT/(MCHT+DMBPH) ratio are significantly higher than the values of CHB/(CHB+BP) ratio, indicating overwhelming HYD activity in HDS of 4,6-DMDBT. Newly developed RePd aerogel catalysts used in this work exhibit outstanding catalytic activity and could represent an interesting opportunity for improvement of hydrogenation of large molecules, which normally occur in heavy petroleum fractions.

Acknowledgements: Financial support by the Ministry of Education and Science of the Republic of Serbia (Contract No. 451-03-68/2022-14/200135) and Institutional funding of the Faculty of Technology and Metallurgy, University of Belgrade is gratefully acknowledged.

REFERENCES

[1] McGuiness L, Nunes MD, Kroes F, Chai I. Automated analysis of bauxite exploration drill hole samples by diffuse reflectance Fourier transform infrared (FTIR) spectroscopy. In: *Proceedings of the 7th International Alumina Quality Workshop*. Australia, 2005; 187–192.

[2] Authier-Martin M, Forte G, Ostap S, See J. The mineralogy of bauxite for producing smelter-grade alumina. *JOM* 2001; *53*(12) :36–40. https://doi.org/10.1007/s11837-001-0011-1

[3] Nechitailov A P, Suss AG, Zhilina TI, Belanova E A. New method of analyzing bauxites to determine their main components and impurities. *Metallurgist* 2008; 52(11): 625–632. https://doi.org/10.1007/s11015-009-9104-9

[4] Blagojevic D, Lazic D, Keselj D, Skundrić B, Dugic P, Ostojic G. Determining the content of silicon dioxide in bauxites using X-ray fluorescence spectrometry. *Iran. J. Chem. Chem. Eng* 2019; 38(4). https://doi.org/10.30492/IJCCE.2019.34231

[5] Ostojic G, Lazic D, Zeljkovic S. Determination of the iron oxide content in bauxite: comparing ICP-OES with UV-VIS and volumetric analysis. *Chem. Pap.* 2020; 75(1): 389-396. https://doi.org/10.1007/s11696-020-01305-z

[6] Idris N, Lahna K, Syamsuddin F, Ramli M. Study on Emission Spectral Lines of Iron, Fe in LaserInduced Breakdown Spectroscopy (LIBS) on Soil Samples. *J. Phys. Conf. Ser* 2017; 846(012020). https://doi.org/10.1088/1742-6596/846/1/012020

[7] Carvalho AAC, Alves VC, Silvestre DM, Leme FO, Oliveira PV, Nomura CS. Comparison of FusedGlass Beads and Pressed Powder Pellets for the Quantitative Measurement of Al, Fe, Si and Ti in Bauxite by Laser Induced Breakdown Spectrometry (LIBS). *Geostand*. *Geoanal. Res.* 2017; 41(4): 585–592. https://doi.org/https://doi.org/10.1111/ggr.12173

[8] Fahad M, Sajjad A, Shah KH, Shahzad A, Abrar M. Quantitative elemental analysis of high silica bauxite using calibration-free laser-induced breakdown spectroscopy. *Appl. Opt.* 2019; 58(27): 7588-7596. /https://doi.org/https://doi.org/10.1364/AQ.58.007588

[9] Upendra S, Mishra RS. Simultaneous multielemental analysis of alumina process samples using inductively coupled plasma spectrometry (ICP-AES*). Anal. Chem.: Indian J.* 2012; 11(1). https://www.tsijournals.com/articles/simultanious-multielemental-analysis-of-alumina-process-samples-using-inductively-coupled-plasma-spectrometry.pdf

[10] Murray RW, Miller DJ, Krys KA. Analysis of major and trace elements in rocks, sediments, and interstitial waters by inductively coupled plasma-atomic emission spectrometry (ICP-AES). *ODP Tech. Note*, 2000; 29. https://doi.org/10.2973/ODP.TN.29.2000

[11] SPECTRO - Smart Analyzer Vision Software, Online-Help vers. 5.01.09XX. Spectro Analytical Instruments GmbH. 2012

[12] Giavarina D. Understanding Bland Altman analysis. *Biochem. Medica* 2015; *25*(2), 141–151. https://doi.org/10.11613/BM.2015.015

[13] Bilić-Zulle L. Comparison of methods: Passing and Bablok regression. *Biochem. Medica* 2011; 21 (1): 49–52. https://doi.org/10.11613/bm.2011.010

[14] Medcalc manual, https://www.medcalc.org/manual/mountain-plot.php, Accessed May 23rd 2020

[15] Linsinger T. Comparison of a measurement result with the certified value. Application Note 1, European Reference Materials. 2010; 1–2.

[16] Certificate of Analysis, Standard Reference Material 697, bauxite Dominican, National Institute of Standards and Technology. 1991

[17] Liberatore PA. Determination of Majors in Geological Samples by ICP-OES*:* Vol. ICP-AES Inst. 1993; 12 https://www.colby.edu/chemistry/CH332/laboratory/Geo-ICP-protocol2.pdf

[18] Hauptkorn S, Pavel J, Seltner H. Determination of silicon in biological samples by ICP-OES after non-oxidative decomposition under alkaline conditions. *Fresenius. J. Anal. Chem* 2001; 370**:** 246–250. https://doi.org/10.1007/s002160100759

[19] US. EPA Method 6010D (SW-846): Inductively coupled plasma-atomic emission spectrometry. Washington, DC, USA, 2014. https://www.epa.gov/esam/epa-method-6010d-sw-846-inductively-coupled-plasma-atomic-emission-spectrometry
[20] Simundic AM. Statistical analysis in method comparison studies-Part one. 2016; www.acutecaretesting.org
[21] AOAC (American Association Of Official Analytical Chemists), *Appendix F : Guidelines for Standard Method Performance Requirements.* 2016. https://www.aoac.org/resources/guidelines-for-standard-method-performance-requirements/
[22] Taftazani A, Roto R, Ananda NR, Murniasih S. Comparison of NAA XRF and ICP-OES Methods on Analysis of Heavy Metals in Coals and Combustion Residues. *Indones. J. Chem.* 2017; 17(2): 228–237. https://doi.org/10.22146/ijc.17686
[23] Rüdel H, Kösters J, Schörmann J. *Determination of the Elemental Content of Environment Sample using ICP-OES, Guidelines for Chemical Analysis*, Fraunhofer Institute for Molecular Biology and Applied Ecology, Schmallenberg, 2007. https://www.ime.fraunhofer.de/content/dam/ime/en/documents/AE/SOP_ICP-OES_en.pdf
[24] Amorin A, *Determination of major and minor elements in HF-digested soil samples using an Agilent 5110 ICP-OES*, application note, Agilent Technologies.Inc. 2019. https://www.agilent.com/cs/library/applications/application_inert_sample_chamber_icp-oes_5110_5994-1213en_us_agilent.pdf
[25] Krishna AK, Murthy NN, Govil PK. Multielement Analysis of Soils by Wavelength-Dispersive X-ray Fluorescence Spectrometry. *At*. Spectrosc 2007; 28(6): 202–214. https://www.researchgate.net/profile/Keshav-Krishna/publication/233786687_Multielement_Analysis_of_Soils_by_Wavelength-Dispersive_X-ray_Fluorescence_Spectrometry/links/57ecd91a08aebb1961ffc510/Multielement-Analysis-of-Soils-by-Wavelength-Dispersive-X-ray-Fluorescence-Spectrometry.pdf

Desulfurizacija dibenzotiofena i 4,6 – dimetildibenzotiofena procesom hidrogenovanja uz korišćenje RePd–TiO_2/SiO_2 aerogel katalizatora: proračun kinetičkih parametara i simulacijaprocesa

Dragana Prokić-Vidojević[1], Sandra B. Glišić[2], Radojica Pešić[2] i Aleksandar M. Orlović[2]

[1]*Vojno tehnički institut (VTI), Ratka Resanovića 1, 11132 Beograd, Srbija*
[2]*Univerzitet u Beogradu, Tehnološko-metalurški fakultet, Karnegijeva 4, 11000 Beograd, Srbija*

(Naučni rad)

Izvod

Re/Pd-TiO_2/SiO^2 aerogel katalizatori su sintetizovani korišćenjem sol-gel metode i natkritičnog sušenja u višku rastvarača, i njihova katalitička aktivnost je ispitana u reakcijama hidrodesulfurizacije (HDS) dibenzotiofena (DBT) i 4,6-dimetildibenzotiofena (4,6-DMDBT). Oba Re/Pd katalizatora, dobijena sa ili bez mezitilena u procesu sinteze, su pokazala povećan stepen konverzije, za 70 %, u reakciji hidrodesulfurizacije 4,6-DMDBT u poređenju sa konvencionalnim Co/Mo katalizatorom koji se koristi u procesima hidroobrade. Ova zapažanja, veći stepen konverzije teško reagujućih 4,6-DMDBT u procesu hidroobrade, su značajna za dobijanje nisko-sumpornih dizel goriva (engl. ultra-low sulphur diesel fuels, ULSD). Kvantitativna analiza produkata hidrogenovanja DBT i 4,6-DMDBT, uključujući međuproizvode, izvedena je tehnikom gasne hromatografije – masene spektrometrije (engl. gas chromatography–mass spectrometry, GC-MS). Eksperimentalna reakcija je izvedena na 630 K i 60 bar u šaržnom katalitičkom reaktoru. Eksperimentalni podaci su korišćeni u okviru Hagen-Vatson (Hougen-Watson) kinetičkog modela koji opisuje proces hidrodesulfurizacije DBT i 4,6-DMDBT na σ i τ aktivnim centrima. Kinetički parametri su određeni korišćenjem numeričkih optimizacionih metoda, genetski algoritam simultano sa funkcijom minimuma odstupanja, i dobijeni rezultati pokazuju dobro slaganje sa eksperimentalnim podacima. Vrednosti izračunatih kinetičkih parametara kao i vrednosti selektivnosti (tj. odnosa metilcikloheksiltoluena i dimetilbifenila kao MCHT/(MCHT+DMBPH)) su potvrdile da je hidrogenovanje dominantni reakcioni put za hidrodesulfurizaciju 4,6-DMDBT. Potencijalne prednosti korišćenja Re/Pd aerogel katalizatora za konverziju 4,6-DMDBT potvrđene su i rezultatima uporednih simulacija ovog i konvencionalnog Co/Mo katalizatora.

Ključne reči: Aerogel katalizator; hidrodesulfurizacija; 4,6-DMDBT; Hagen-Vatson kinetički model; kinetički parametari